Correlation between Phase Behavior and Electrical Conductivity of 10 mol% Y-Doped BaZrO$_3$:

An Anomalous Dispersion Effect-Aided Synchrotron Radiation XRD Study Combined with

TEM Observation and Electrochemical Analysis

Donglin Han [*], Tetsuya Uda [*]

Department of Materials Science and Engineering, Kyoto University,

Yoshida Honmachi, Sakyo-ku, Kyoto 606-8501, Japan

* Corresponding authors: Donglin Han (han.donglin.8n@kyoto-u.ac.jp)

and Tetsuya Uda (uda_lab@aqua.mtl.kyoto-u.ac.jp)

Abstract

Y-doped $BaZrO_3$ (BZY) has high proton conductivity, and is a promising electrolyte candidate for fuel cells and electrolysis cells at intermediate temperature range. However, the conductivity of BZY has large discrepancy in literature. Especially for $BaZr_{0.9}Y_{0.1}O_{3-\delta}$ (BZY10), the reported bulk conductivity varies in the range of more than two orders. With the aim to reveal the reason, in this work, we conducted a synchrotron radiation XRD analysis on BZY10. The X-ray was adjusted to 17.027 keV to approach the Y-K absorption edge (17.037 keV), anomalous dispersion effect was thereby activated for a precise distinction between Zr and Y. High resolution STEM observation and electrochemical measurements were also performed. Assisted with these experimental results, Rietveld refinement with greatly improved quality was thereby available to generate precise information on both the phase behavior and crystal structure. The results revealed that the BZY10 samples after sintering at 1600 °C for 8 to 200 h have a bimodal microstructure. They were not single phases, but mixtures of two perovskite phases different slightly in Y contents. The Y contents in the two phases after sintering for 8 h were about 12.3 and 8.7 mol%, respectively, and finally became 10.6 and 9.2 mol%, respectively, after sintering for 200 h. In addition, partition of Y over both the Ba and Zr sites was not suggested, although small Ba-deficiency around 0.05 formed in the sample sintered for 40 h or longer. But notably, the formation of the Ba vacancies is reasonably to be believed as the possible reason for the decrease in bulk and also grain boundary conductivities.
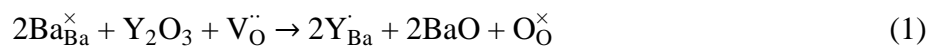
1. Introduction

Due to its clean and sustainable feature, hydrogen is expected to play a vital role as an energy medium to construct the energy framework of future society. Fuel cells are one type of efficient energy conversion devices which directly produce electricity by consuming hydrogen. If they work reversely, namely as electrolysis cells, hydrogen is generated. A combination of fuel cells and electrolysis cells thereby offers a flexible solution on energy production, storage and consumption, and is regarded to be an important and effective component in the hydrogen-based society. The most vital part in both the fuel cells and electrolysis cells is the electrolyte, whose properties almost determine the selection criteria of other components and operation condition. Currently, oxide ion conductive ceramic (*e. g.*, Y-stabilized ZrO_2 (YSZ)) and proton conductive polymer (*e. g.*, Nafion) are two main types of electrolyte. However, the former one needs very high operation temperatures (800 - 1000 ^oC) for sufficient oxide ion conductivity (> 0.01 Scm^{-1}), inducing risk on material compatibility and long-term stability [1, 2]. Whereas the latter one is poorly thermal resistive, and expensive platinum is still essential to provide sufficient catalytic activity at the low operation temperature, typically around 80 ^oC [3, 4].

Operating at an intermediate temperature range (400 – 700 ^oC), the cells using proton conductive ceramic-type electrolyte offer a promising solution. Y-doped $BaZrO_3$ (BZY) is presently the most attractive electrolyte material, since its proton conductivity exceeds 0.01 Scm^{-1} even around 500 ^oC. [5-8] However, literature data on the conductivity of BZY show obvious discrepancy. Especially for

3

BaZr$_{0.9}$Y$_{0.1}$O$_{3-\delta}$ (BZY10), as shown in **Figure 1(a)** and **Table 1**, their reported bulk (intra-grain)

conductivities [7-12, 17] vary more than two orders of magnitude.   In our previous work, we observed

that the bulk conductivity (σ_{bulk}) of BZY10 correlated with sintering time at 1600 °C; that is, σ_{bulk}

deceased by about one order of magnitude when the sintering time was increased from 24 h to 40 –

200 h. [8]   Azad, *et al*. also reported the dependence of σ_{bulk} on the fabrication route of BZY10.

Formation of Ba-deficiency is one common reason lowering the conductivity of BZY [18, 19], but Azad,

et al. considered the difference in site occupancy of yttrium (Y) as the reason for their sample, and

demonstrated that Y cations occupy the Ba-site in a more conductive BZY10 phase. [10]   But, it seems

to be questionable, since as given in eq. 1, substituting the divalent Ba cations (Ba$_{Ba}^{\times}$) with the trivalent

Y cations (Y$_{Ba}^{'}$) results in the consumption of oxide ion vacancies (V$_{O}^{\cdot\cdot}$), which is detrimental to the

hydration reaction (eq 2), and decreases the concentration of charge carriers of protons (OH$_{O}^{\cdot}$).   The

conclusion of Azad, *et al*. was generated through neutron diffraction analysis, but questionably, based

on a rather arbitrary assumption that their BZY10 samples were compositionally homogenous.

However, in fact, the diffraction patterns of the samples showed obvious feature of two co-existing

perovskite phases. [10]

$$2Ba_{Ba}^{\times} + Y_2O_3 + V_O^{\cdot\cdot} \rightarrow 2Y_{Ba}^{'} + 2BaO + O_O^{\times} \tag{1}$$

$$H_2O + V_O^{\cdot\cdot} + O_O^{\times} \rightarrow 2OH_O^{\cdot} \tag{2}$$

Revealing the origin of the conductivity discrepancy of Y-doped BaZrO$_3$ not only gives profound

understanding on the nature of material, but also provides important information on the promotion of

its practical application, including improving the cell performance and long-term stability. Therefore, it appears to be highly necessary to conduct a detailed re-investigation on the BZY10 system to comprehensively correlate a couple of parameters, including the electrical conductivity, phase behavior, crystal structure, and local composition. With such aim, in this work, scanning transmission electron microscopy (STEM) observation coupled with energy dispersive X-ray spectroscopy (STEM-EDS) point analysis leads to the success in distinguishing the phases which are only slightly different in compositions. Benefited from such accurate compositional information, synchrotron radiation X-ray diffraction (XRD) analysis and Rietveld refinement was performed with greatly improved quality.

It has to be noted that Zr and Y can hardly be distinguished by XRD analysis using ordinary X-ray source (*e. g*, Cu $K\alpha$), since as shown in **Figure 2**, their scattering factors (f_n, as given in eq. 3) are very close due to their adjacent position in the periodic table. In eq. 3, subscript n represents the element (Ba, Y or Zr), θ is the incident angle, λ and E are the wavelength and energy of the X-ray, respectively. In this work, the energy of the synchrotron radiation X-ray was adjusted carefully to be 17.027 keV, approaching the Y-K absorption edge (17.037 keV). With such special X-ray energy, as shown in **Figure 2(c)**, the difference in the real part ($f_n'(E)$) of the anomalous dispersion term ($f_n'(E) + i f_n''(E)$) between Y and Zr increases, which therefore enables more precise analysis of crystal structure, especially the site occupancy of Y.

$$f_n = f_{n,0}(\sin\theta/\lambda) + f_n'(E) + i f_n''(E) \qquad (3)$$

5

2. Experimental

2.1 Material Preparation

The $BaZr_{0.9}Y_{0.1}O_{3-\delta}$ (BZY10) samples were prepared by a conventional solid state reaction method. Starting materials of $BaCO_3$ (Wako Pure Chemical Industries, Ltd., 99.9%), ZrO_2 (Tosoh Corporation, 98.01%), Y_2O_3 (Shin-Etsu Chemical Co., Ltd., 99.9%) were mixed at the desired ratio, and ball-milled in 2-propanol as the solvent for 24 h. After being pelletized under 9.8 MPa, the sample were heat-treated at 1000 $^{\circ}$C for 10 h. Then, the sample was pulverized and ball-milled for 10 h, and pelletized under 9.8 MPa again, with a subsequent heat-treatment at 1300 $^{\circ}$C for 10 h for synthesizing. The as-synthesized samples were ball-milled for 100 h to be pulverized into powder-likes samples with the grain size around 100 nm, and mixed with a binder (NCB-166, DIC Corporation, Tokyo, Japan). After being pressed at 392 MPa into pellets with thickness and diameter around 1 mm and 11 mm, respectively, the samples were heat-treated at 600 $^{\circ}$C for 8 h to remove the binder. Finally, the resulting pellets were buried in sacrificial powder composed of 99 wt% as-synthesized BZY10 and 1 wt% $BaCO_3$, and subjected to sintering at 1600 $^{\circ}$C in pure oxygen atmosphere. The heating rate was 4.17 $^{\circ}$Cmin^{-1} from room temperature to 1000 $^{\circ}$C, and 3.33 $^{\circ}$Cmin^{-1} from 1000 to 1600 $^{\circ}$C. The samples were quenched in ambient atmosphere after the keeping at 1600 $^{\circ}$C for 8, 24, 40, 70, 100 and 200 h.

2.2 Characterization

Chemical compositions were determined by inductively coupled plasma atomic emission spectroscopy (ICP-AES) with SPS4000 (Seiko Instruments Inc., Chiba, Japan).   Microstructures were observed by scanning transmission electron microscopy (STEM) with JEOL JEM-2100F.   Energy dispersion X-ray spectroscopy (STEM-EDS, JEOL JED-2300) point analysis was applied to determine the local composition of individual grains.   Samples for STEM observations were thinned by an argon ion (Ar^+) beam using a JEOL EM-09100IS Ion Slicer.   Relative density was measured with Archimedes method.

Powder X-ray diffraction (XRD) measurements were performed at SPring-8 synchrotron radiation facility (Hyogo, Japan) at beamline BL19B2 with the approval of the Japan Radiation Research Institute (JASRI) (Proposal No. 2018A1782).   The X-ray energy was adjusted to 17.027 keV, close to the Y-K absorption edge (17.037 keV), to activate the anomalous dispersion effect.   Powder samples were filled into glass capillaries with the outer diameter of 0.3 mm (Hilgenberg GmbH, Malsfeld, Germany).   And each sample was exposed to X-ray radiation for 60 s to collect the XRD patterns.   Rietveld refinement was performed by using GSAS-II [22].

Conductivity measurements of the pellet-like samples with sputtered platinum (Pt) electrodes were performed in wet H_2 atmosphere with the partial pressure of water vapor kept at 0.05 atm.   Pt plates wrapped with silver mesh were used as current collector.   Pt wire was used to lead the current to a frequency response analyzer (Solartron SI 1260, Solartron Analytical, Farnborough, UK).   The

sample was firstly held at 700 $^{\circ}$C for more than 18 h for sufficient hydration until the impedance spectra stopped shifting, and then, cooled gradually from 700 to 100 $^{\circ}$C at 0.2 $^{\circ}$Cmin-1 with the impedance spectra collected with an interval of 50 min in the frequency range from 10 Hz to 7 MHz with applied voltage of 100 mV.   The spectra were lately analyzed using a commercial software ZView (Scribner Association Inc., NC, USA).

3. Results

3.1 Electrical Conductivity

To check the consistency with the conductivities of the BZY10 samples sintered at 1600 $^{\circ}$C for 24, 40, 70, 100 and 200 h, which were reported in our previous work [8], we here additionally measured the conductivity of the sample sintered for 8 h.   **Figure 3** shows representative impedance spectra collected at 200 $^{\circ}$C in wet H_2.   An equivalent circuit composed of two series connected components of parallel resistance and capacitance elements [23, 24] was used to simulate the impedance spectra, and the semicircles belonging to the contribution of bulk (intra-grain) and grain boundary were separated by their specific capacitances around 10^{-11} F and 10^{-9} F, respectively.   The conductivities were then calculated with the geometric parameters.

The bulk conductivity (σ_{bulk}), as shown in **Figure 1(a)**, of the BZY10 sample sintered at 1600 $^{\circ}$C for 8h shows good consistency with our previous report; that is, it is close to that of the sample sintered for 24 h, and is higher than those of the samples sintered for longer time (40 – 100 h).   Regarding the

8

grain boundary (σ_{GB}) and total conductivities (σ_{total}), as shown in **Figures 1(b)** and **1(c)**, extending the

sintering time from 8 h to 24 h results in an improvement in both σ_{GB} and σ_{total}, possibly due to the

grain growth and improvement of relative density from 89.23 % to 92.90 % as given in **Table 2**.

However, although extending the sintering time over 24 h further increases the relative density (*e. g.*,

96.86 % for sintering for 100 h), it does not further improve σ_{GB}.   Obviously, the sample sintered for

24 h has the highest σ_{GB} and σ_{total}.   The reason might be due to the severe loss of BaO from grain

boundary when the sample was kept at 1600 °C too long, which will be discussed later on.

3.2 Microstructure Observation

A bimodal microstructure with the feature of co-existence of large and fine grains was confirmed for

all the BZY10 samples which was sintered at 1600 °C for 8 to 200 h in our previous work by electron

probe micro analysis (EPMA) [8].   However, the resolution of EPMA is not sufficient to show a clear

contour of the fine grains.   In this work, the individual fine grains were identified clearly by STEM

observation, as shown in **Figure 4**.   The fine grains have the size typically not larger than 100 nm in

the sample sintered for 8 h, but grow with the increasing sintering time, and turn to be around 200 nm

after sintering for 100 h.   In addition, the size of the large grains, which is of the micrometer order,

also increases clearly by extending the sintering time.

3.3 Composition Analysis

Average compositions of the samples determined by ICP-AES are listed in **Table 2**. All the samples were embedded in the BZY10 – 1 wt% $BaCO_3$ sacrificial powder to suppress the evaporation of BaO during sintering at 1600 $^{\circ}$C [18], but such method seems to only work for relatively short time of 8 and 24 h, since formation of Ba-deficiency was confirmed in the samples heated for 40 h and longer.

To determine the accurate local composition of individual grains, especially that of fine grains which are only 100 – 200 nm in diameter, we adopted STEM-EDS point analysis with the spot size about 1 nm (an example is given in **Figure S1**). As shown in **Figure 5**, the data present a clear impression on how the large and fine grains distribute compositionally. The large grains have obviously higher Y content than the fine grains, after sintered at 1600 $^{\circ}$C for 8 h and 24 h. And with the sintering time increasing to 40 h and longer, such compositional difference reduces, but still, one can confirm that the data spots belonging to the large grains distribute in the slightly Y-rich side.

To visualize quantitatively the compositional difference, average compositions of the large and fine grains were calculated and listed in **Table 2**, and the Y and Ba contents are plotted in **Figure 6**. In the sample after sintering at 1600 $^{\circ}$C for 8 h, the large and fine grains have the Y content (x, in $BaZr_{1-x}Y_xO_{3-\delta}$) of 0.123 and 0.087, respectively, indicating quite large difference in the Y content in these two types of grains. With the increase in the sintering time, the Y content starts to approach with each other. And when the sintering time was extended to 70 h, the Y contents in the large and fine grains are 0.107 and 0.095, respectively. Further extending the sintering time to 100 and 200 h seems

to influence little on the Y content in these two type of grains.   Regarding the Ba content, the samples

sintered at 1600 °C for 8 and 24 h has the Ba content close to unity.   However, when the sintering

time was 40 h or longer, quite obvious Ba-deficiency forms.   The Ba content in the both the large and

fine grains are typically around 0.95.

3.4 Synchrotron Radiation XRD Patterns

The XRD patterns collected using the synchrotron radiation X-ray with the incident energy of 17.027

keV, are shown in **Figure 7**.   The diffraction peaks of the as-synthesized BZY10 sample show a broad

and asymmetric appearance with a shoulder at the relatively small angle side, which is due to the large

inhomogeneity of composition, especially the Y content [25].   The heat-treatment condition is the

reason, since neither the temperature (1300 °C) nor the time (10 h) is sufficient for a complete reaction.

In addition, some starting materials, including $BaCO_3$, ZrO_2, and Y_2O_3, also remained in such as-

synthesized sample. [25, 26]

When the sample was sintered at 1600 °C for 8 h, as shown in the insets of **Figure 7**, all the reflections

exhibit the feature of two peaks, indicating the co-existence of two cubic perovskite phases, rather than

lattice distortion from the cubic perovskite crystal structure.   With the sintering time extending to 24

h and longer, the diffraction peak at the low angle side turns to be sharper, implying improvement in

crystallinity.   The two peaks approaching with each other, but do not merge to a complete single

symmetric peak even after the sample was kept at 1600 °C for 200 h.

11

3.5 Rietveld Refinements

Both the results of STEM-EDS point analysis and synchrotron radiation XRD measurements indicate that the BZY10 samples sintered at 1600 °C for 8 to 200 h are not of a single phase, but comprise of two perovskite phases actually.   Since the six-coordinated radius of Y(III) cations (0.900 Å) is larger than that of Zr(IV) cations (0.72 Å) [27], the lattice constant increases with the increasing Y content, if the sample is stoichiometric or only slightly Ba-deficient [7, 8, 19, 28, 29].   Therefore, the compositions of large grains and fine grains, which are relatively Y-rich and Y-poor as shown in **Table 2**, were assigned to the phases with large and small lattice constants, respectively, by fixing the cation ratio among Ba, Zr and Y.   And two cubic perovskite structure ($Pm\bar{3}m$) models [29-31] were used in Rietveld refinements to simulate these two phases.   In addition, Ba cations and Zr cations were fixed in the A and B sites of the perovskite-type (ABO$_3$) structure since it is much more energetically stable [32], and only Y was set to be movable across A and B-sites.

The fitting results of (222) and (631) reflections are shown in **Figure 8** and **Figure 9** to give a direct impression on how well the XRD patterns were fitted.   Fitting results of entire XRD patterns are given in the Supporting Material.   One can see that the calculated profiles almost overlap with the measured ones.   And the R_{wp} factor is between 6.65 and 8.25%, indicating that the Rietveld refinements were performed with reasonably good quality.   The fitting results are summarized in **Table 3**, and the phase fractions and lattice constants are also plotted in **Figure 10**.   The fractions of both the two phases are close to 50 wt%, and change only slightly with the increase of sintering time.

12

The lattice constants of the two phases behave similarly as the Y content; that is, they turn to be close with each other obviously during sintering for 8 to 40 h. And the difference in either the lattice constant or the Y content between the two phases changes only slightly when the sintering time varies between 70 and 200 h. Notably, another important finding is that, we did not confirm the occupation of Y into the Ba-site for all the samples as shown in **Table 3**, opposing to the conclusion of Azad, *et al*. [10]

4. Discussion

In the Y-doped $BaZrO_3$ system with the Ba content close to unity, or only small Ba-deficiency, Y seems to be unable to partition over both the Zr and Ba sites. Giannici, *et al*. found no evidence of Y in the Ba-site through an extended X-ray absorption fine structure (EXAFS) analysis on nominally stoichiometric $BaZrO_3$ doped with 6 and 15 mol% Y [31]. Our recent synchrotron radiation XRD study on 20 mol% Y-doped $BaZrO_3$ with only 0.03 Ba-deficiency also achieved a similar conclusion [29]. And still, no occupation of Y on the Ba-site was confirmed in the nominally stoichiometric 10 mol% Y-doped $BaZrO_3$ system in this study. As far as we know, Y is only capable to be driven into the Ba-site in the system containing large Ba-deficiency and large Y content. For example, we found that a perovskite phase with the composition of Ba : Zr : Y = 42.53 : 31.61 : 25.86 at% has the actual formula of $(Ba_{0.851}Y_{0.149})(Zr_{0.632}Y_{0.368})O_{3-\delta}$ in the sample with the average composition of $Ba_{0.9}Zr_{0.8}Y_{0.2}O_{3-\delta}$ [29].

Referring to the reason leading Azad, *et al*. to the conclusion that Y occupies the Ba-site, it possibly relies on their arbitrary assumption that the sample is compositional homogeneous without performing detailed measurement. Such overlooking on the inhomogeneity in composition is easy to make, since in fact, we also found it quite challenging to distinguish the two co-existing phases whose compositions are very close. However, the evidence of the co-existence of these phases is further strengthened from the correlated parameters between different experiments, for example, lattice constants and Y-contents of the two phases, as shown in **Figure 6** and **Figure 10**. These two parameters were determined with two almost independent methods, but behave in a similar way with the increasing sintering time. Furthermore, in general, the one with larger Y content has a larger lattice constant, agreeing with the common knowledge on this system [7, 8, 19, 28, 29]. But, it should be noted that the area which is thin enough for the STEM observation is very limited, resulting in the uncertainty on whether the sampling number is enough. For example, we were only capable to collect the composition of seven large grains in the sample sintered for 8 h, and obviously, these data scatter in certain degree. However, since the weight ratio of the large grains ($Ba_{1.001}Zr_{0.877}Y_{0.123}O_{3-\delta}$) and fine grains ($Ba_{1.002}Zr_{0.913}Y_{0.087}O_{3-\delta}$) were estimated to be 49.70 and 50.30 wt%, respectively, the average Y content should be around 10.5 mol%, very close to 10 mol% which was determined by ICP-AES measurement. So, increasing the sampling number by preparing new samples will enhance the reliability of the data from the statistical viewpoint, but the tendency of the compositional difference between these two phases will not change.

14

Occupying the Ba-site with the Y cations is not the reason for the change of conductivity with the sintering time.   From the STEM-EDS point analysis results provided in this work, loss of BaO due to heating at such high temperature (1600 $^\circ$C) is more possible to be the reason, although we previously did not think so [8].   The Ba content in the intra-grain of the samples sintered at 8 and 24 h is almost unity, but decreased to around 0.95 when the sintering time was extended to 40 and even longer.   And Ba vacancies in general decreases the bulk conductivity [8, 13, 19, 33].   In addition, Ba-deficiency also possibly induces the formation of stacking faults in some samples with special compostion [33, 34], which possibly blocking the movement of protons.   Compared with some other compositions (*e. g.*, $BaZr_{0.85}Y_{0.15}O_{3-\delta}$ and $BaZr_{0.8}Y_{0.2}O_{3-\delta}$), it is more difficult for $BaZr_{0.90}Y_{0.10}O_{3-\delta}$ to get densified through sintering [8].   The relative large amount of pores remained during the sintering process increase the surface area contacting with gas, promoting the loss of BaO through evaporation.   This will also result in the formation of Ba-deficiency along the grain boundary, and therefore decreases the grain boundary conductivity.

The sintering behavior of $BaZr_{0.90}Y_{0.10}O_{3-\delta}$ appears to be quite special.   Two perovskite phases form at the initial stage of the sintering, and gradually approach with each other compositionally, but simultaneously, the weight fraction of each phase was kept nearly steady around 50 wt%.   An inter-diffusion of Y and Zr between these two phases should be the rate-limiting step.   As shown in **Figure S9**, even the sample with a close composition ($BaZr_{0.88}Y_{0.12}O_{3-\delta}$) has the grains growing uniformly after sintering at 1600 $^\circ$C for 100 h.   If we assume that $BaZr_{0.88}Y_{0.12}O_{3-\delta}$ can reach equilibrium faster

than $BaZr_{0.90}Y_{0.10}O_{3-\delta}$ before losing BaO significantly, and the BaO loss reduces the ability of grain boundary to move for grain growth, the phenomenon seems to be explainable.   However, the driving force to form two perovskite phases is also unknown.

Although the samples prepared in this study exhibit a bimodal microstructure, as shown in **Table 1**, grain growth with uniform size was also reported by Kjølseth, *et al*. (1650 ℃) [11], Duval, *et al*. (1720 and 2200 ℃) [12], which were prepared with the temperature higher than 1600 ℃.   The results imply the dependence of phase behavior of $BaZr_{0.90}Y_{0.10}O_{3-\delta}$ on temperature.   We will report a detailed investigation on the phase behavior of $BaO – ZrO_2 – YO_{1.5}$ in near future.

5. Conclusions

In this work, synchrotron radiation XRD analysis using the X-ray with the energy of 17.027 keV, which is close to the Y-*K* absorption edge, was conducted on $BaZr_{0.9}Y_{0.1}O_{3-\delta}$ (BZY10).   Benefited from such special X-ray energy, anomalous dispersion effect was activated to enable a precise distinction between Zr and Y.   Rietveld refinement was performed with good quality by using the information obtained from high resolution STEM observation and electrochemical measurements. The results revealed that the BZY10 samples after sintering at 1600 ℃ for 8 to 200 h have a bimodal microstructure.   They were not single perovskite phases, but mixtures of two phases with cubic perovskite structures which are different in Y contents, regardless of the time kept at 1600 ℃.   The Y contents for the two phases in the sample sintered for 8 h were about 12.3 and 8.7 mol%, respectively,

and approach with each other with the increasing sintering time, and finally became 10.6 and 9.2 mol% after sintering for 200 h.   Furthermore, we did not find Y partition over both the Ba and Zr sites, although small Ba-deficiency around 0.05 formed in the sample sintered for 40 h or longer.   But in fact, such formation of Ba vacancies is much more reasonable to be the reason for the decrease in bulk and also grain boundary conductivities, indicating the necessity to maintain the stoichiometry of the composition for high conductivity.

Acknowledgements

Supporting Information Available: example of STEM-EDS point analysis on BZY10 sintered at 1600 $^{\circ}$C for 24 h, and results of STEM-EDS point analysis plotted in full scale (0 – 100 at%), and results of Rietveld refinement on entire XRD patterns.

References

(1) Ormerod, R.M., Solid Oxide Fuel Cells, *Chem. Soc. Rev*. **2003**, *32*, 17 - 28.

(2) Jacobson, A.J., Materials for Solid Oxide Fuel Cells, *Chem. Mater*. **2010**, *22*, 660 - 674.

(3) Steele, B.C.H.; Heinzel, A., Materials for Fuel-Cell Technologies, *Science* **2001**, *414*, 345 - 352.

(4) Litster, S.; McLean. G., PEM Fuel Cell Electrodes, *J. Power Sources* **2004**, *130*, 61 - 76.

(5) Yamazaki, Y.; Hernandez-Sanchez, R.; Haile, S.M., High Total Proton Conductivity in Large-Grained Yttrium-Doped Barium Zirconate, *Chem. Mater*. **2009**, *21*, 2755 - 2762.

(6) Pergolesi, D.; Fabbri, E.; D'Epifanio, A.; Di Bartolomeo, E.; Tebano, A.; Sanna, S.; Licoccia, S.; Balestrino, G.; Traversa, E., High Proton Conduction in Grain-Boundary-Free Yttrium-Doped Barium Zirconate Films Grown by Pulsed Laser Deposition, *Nat. Mater.* **2010**, 9, 846-852.

(7) Han, D.; Hatada, N.; Uda, T., Chemical Expansion of Yttrium-Doped Barium Zirconate and Correlation with Proton Concentration and Conductivity, *J. Am. Ceram. Soc*. **2016**, *99*, 3745 - 3753.

(8) Han, D.; Uda, T., The Best Compostion of an Y-Doped $BaZrO_3$ Electrolyte: Selection Criteria from Transport Properties, Microstructure, and Phase Behavior, *J. Mater. Chem. A* **2018**, 6, 18571-18582.

(9) Bohn, H.G.; Schober, T., Electrical Conductivity of the High Temperature Proton Conductor $BaZr_{0.9}Y_{0.1}O_{2.95}$, *J. Am. Ceram. Soc.* **2000**, 83, 768-772.

(10) Azad, A.K,; Savaniu, C.; Tao, S.; Duval, S.; Holtappels, P.; Ibberson, R.M.; Irvine, J.T.S., Structural Origins of the Differing Grain Conductivity Values in $BaZr_{0.9}Y_{0.1}O_{2.95}$ and Indication of Novel Approach to Counter Defect Association, *J. Mater. Chem.* **2008**, 18, 3414-3418.
18

(11) Kjølseth, C.; Fjeld, H.; Prytz, Ø.; Dahl, P.I.; Estournès, C.; Haugsrud, R.; Norby, T., Space-Charge Theory Applied to the Grain Boundasry Impedance of Proton Conducting $BaZr_{0.9}Y_{0.1}O_{3-\delta}$, *Solid State Ionics* **2010**, 181, 268-275.

(12) Duval, S.B.C.; Holtappels, P.; Vogt, U.F.; Pomjakushina, E.; Conder, K.; Stimmung, U.; Graule, T., Electrical Conductivity of the Proton Conductor $BaZr_{0.9}Y_{0.1}O_{3-\delta}$ Obtained by High Temperature Annealing, *Solid State Ionics* **2007**, 178, 1437-1441.

(13) Han, D.; Noda, Y.; Onishi, T.; Hatada, N.; Majima, M.; Uda, T., Transport Properties of Acceptor-Doped Barium Zirconate by Electromotive Force Measurements, *Int. J. Hydrogen Energy* **2016**, *41*, 14897 - 14908.

(14) Kato, K.; Han, D.; Uda, T., Transport Properties of Proton Conductive Y-Doped $BaHfO_3$ and Ca or Sr-Substituted Y-Doped $BaZrO_3$, *J. Am. Ceram. Soc*. **2018**, DOI: 10.1111/jace.19546.

(15) Han, D.; Uemura, S.; Hiraiwa, C.; Majima, M.; Uda, T., Detrimental Effect of Sintering Additives on Conducting Ceramics: Yttrium-Doped Barium Zirconate, *ChemSusChem* **2018**, *11*, 4102 – 4113.

(16) Chen. M.; Chen. D.; Wang, K.; Xu, Q., Densification and Electrical Conductivity Behavior of $BaZr_{0.9}Y_{0.1}O_{3-\delta}$ Proton Conducting Ceramics with NiO Additive, *J. Alloys Compd.* **2018**, DOI: 10.1016/j.jallcom.2018.12.090.

(17) Schober, T.; Bohn, H.G., Water Vapor Solubility and Electrochemical Characterization of the High Temperature Proton Conductor $BaZr_{0.9}Y_{0.1}O_{2.95}$, *Solid State Ionics* **2000**, 127, 351-360.

(18) Babilo, P.; Uda, T.; Haile, S.M., Processing of Yttrium-Doped Barium Zirconate for High Proton

Conductivity, *J. Mater. Res*. **2007**, *22*, 1322 – 1330.

(19) Yamazaki, Y.; Hernandez-Sanchez, R.; Haile, S.M.; Cation Non-Stoichiometry in Yttrium-Doped Barium Zirconate: Phase Behavior, Microstructure, and Proton Conductivity, *J. Mater. Chem.* **2010**, *20*, 8158 – 8166.

(20) Cromer, D. T.; Mann, J. B., X-ray Scattering Factors Computed from Numerical Hartree-Fock Wave Functions, *Acta. Cryst*. **1968**, *A24*, 321-324.

(21) Homepage of Research Group for Structural Characterization of Materials, Institute for Advanced Materials Processing, Tohoku University, Japan. (http://res.tagen.tohoku.ac.jp/~waseda/scm/), accessed December 14, 2018.

(22) Toby, B.H.; Von Dreele, R.B., GSAS-II: the Genesis of a Modern Open-Source All Purpose Crystallography Software Package, *J. Appl. Crystallogr.* **2013**, *46*, 544-549.

(23) Haile, S.M.; West, D.L.; Campbell, J., The Role of Microstructure and Processing on the Proton Conducting Properties of Gadolinium-Doped Barium Cerate, *J. Mater. Res*. **1998**, *13*, 1576 - 1595.

(24) Han, D.; Nose, Y.; Shinoda, K.; Uda, T., Site Selectivity of Dopants in $BaZr_{1-y}M_yO_{3-\delta}$ (M = Sc, Y, Sm, Eu, Dy) and Measurement of Their Water Contents and Conductivities, *Solid State Ionics* **2012**, *213*, 2 - 7.

(25) Han, D.; Otani, Y.; Noda, Y.; Onishi, T.; Majima, M.; Uda, T., Strategy to Improve Phase Compatibility between Proton Conductive $BaZr_{0.8}Y_{0.2}O_{3-\delta}$ and Nickel Oxide, *RSC Adv*. **2016**, *6*, 19288 – 19297.

(26) Fang, S.; Wang, S.; Brinkman, K.S.; Su, Q.; Wang, H.; Chen, F., Relationship between Fabrication Method and Chemical Stability of Ni – BaZr$_{0.8}$Y$_{0.2}$O$_{3-\delta}$ Membrane, *J. Power. Sources* **2015**, *278*, 614 – 622.

(27) Shannon, R.D., Revised Effective Ionic Radii and Systematic Studies of Interatomic Distances in Halides and Chalcogenides, *Acta Crystallogr., Sect. A: Phys., Diffr., Theor. Gen. Crystallogr.* **1976**, *A32*, 751 – 767.

(28) Fabbri, E.; Pergolesi, D.; Licoccia, S.; Traversa, E., Does the Increase in Y-Dopant Concentration Improve the Proton Conductivity of BaZr$_{1-x}$Y$_x$O$_{3-\delta}$ Fuel Cell Electrolytes? *Solid State Ionics* **2010**, *181*, 1043 – 1051.

(29) Han, D.; Kishida, K.; Shinoda, K.; Inui, H.; Uda, T., A Comprehensive Understanding of Structure and Site Occupancy of Y in Y-Doped BaZrO$_3$, *J. Mater. Chem. A* **2013**, *1*, 3027 - 3033.

(30) Han, D.; Shinoda, K.; Uda, T.; Dopant Site Occupancy and Chemical Expansion in Rare Earth-Doped Barium Zirconate, *J. Am. Ceram. Soc.* **2014**, *97*, 643 - 650.

(31) Giannici, F.; Shirpour, M.; Longo, A.; Martorana, A.; Merkle, R.; Maier, J., Long-Range and Short-Range Structure of Proton-Conducting Y:BaZrO3, *Chem. Mater.* **2011**, *23*, 2994 - 3002.

(32) Kuwabara, A.; Fisher, C.A.; Moriwake, H.; Oba, F.; Matsunaga, K.; Tanaka, I, *15th International Conference on Solid State Protonic Conductor*, Santa Barbara, USA, 2010.

(33) Han, D.; Kishida, K.; Inui, H.; Uda, T., Substantial Appearance of Origin of Conductivity Decrease in Y-Doped BaZrO$_3$ due to Ba-Deficiency, *RSC Adv*. **2014**, *4*, 31589 – 31593.

(34) Ding, J.; Balachandran, J.; Sang, X.; Guo, W.; Veith, G.M.; Bridges, C.A.; Rouleau, C.M.;

Poplawsky, J.D.; Bassiri-Gharb, N.; Ganesh, P.; Unocic, R.R., Influence of Nonstoichiometry on

Proton Conductivity in Thin-Film Yttrium-Doped Barium Zirconate, *ACS Appl. Mater. Interfaces*
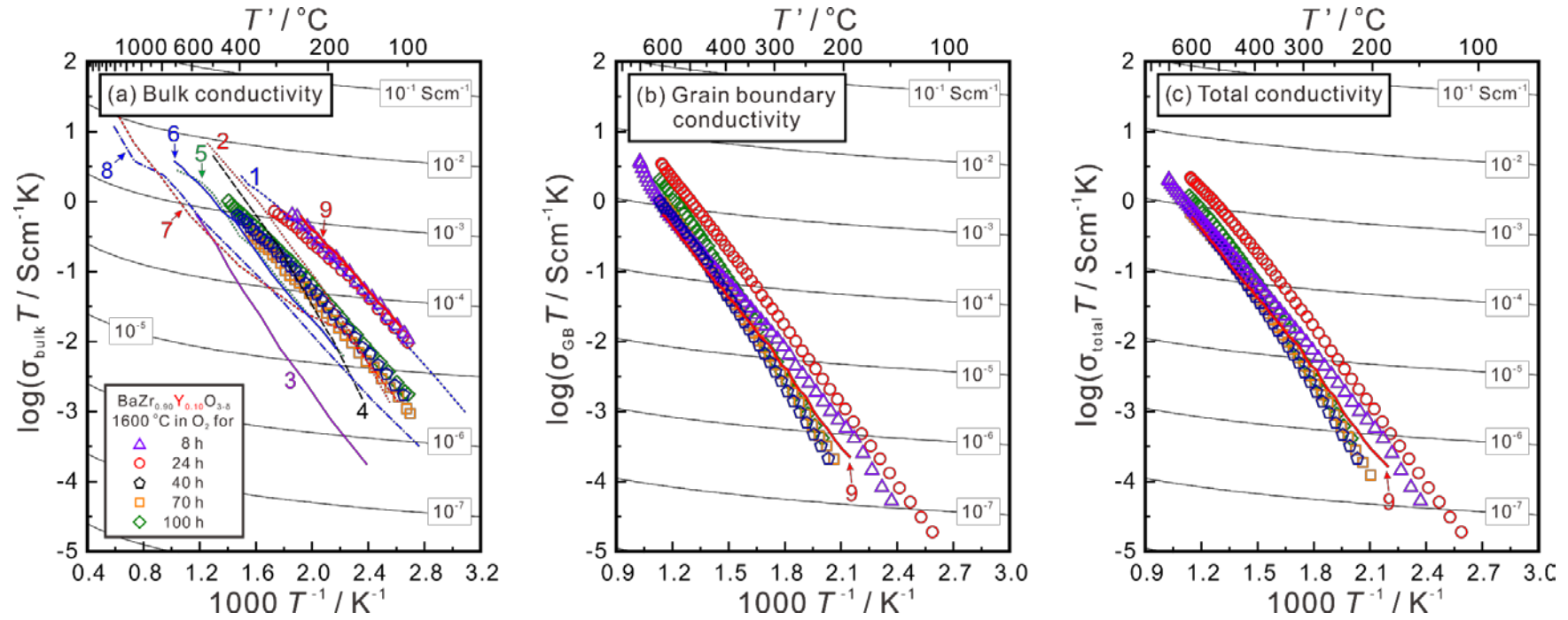
2018, *10*, 4816-4823.

Figure 1 (a) Bulk conductivities, (b) Grain boundary conductivities, and (c) total conductivities of BaZr$_{0.9}$Y$_{0.1}$O$_{3-\delta}$ (BZY10) measured in wet H$_2$

(p_{H_2O} = 0.05 atm). Literature data of the conductivity of BZY10 (1 by Bohn and Schober [9], 2, 3 and 4 by Azad, *et al*. [10], 5 and 6 by Kjølseth, *et al*. [11] , 7 and 8 by Duval, *et al*. [12]), and our previous reported data of the samples sintered in oxygen atmosphere at 1600 °C for 24, 40, 70 or 100 h [7, 8] were also plotted for comparison. The conductivities of the sample sintered at 1600 °C for 8 h were collected in this study. 1, 5, 6, 7 and 8 were measured in wet oxidizing atmophere, and others were measured in wet reducing atmosphere. In oxidizing atmosphere, hole conduction also generates in Y-doped BaZrO$_3$, and becomes obvious at high termperature (*e.g*., > 500 °C). However, at relatively low temperature (e.g. < 500 °C), the transport number of protons is almost unity, regardless of the atmosphere. [13-16]
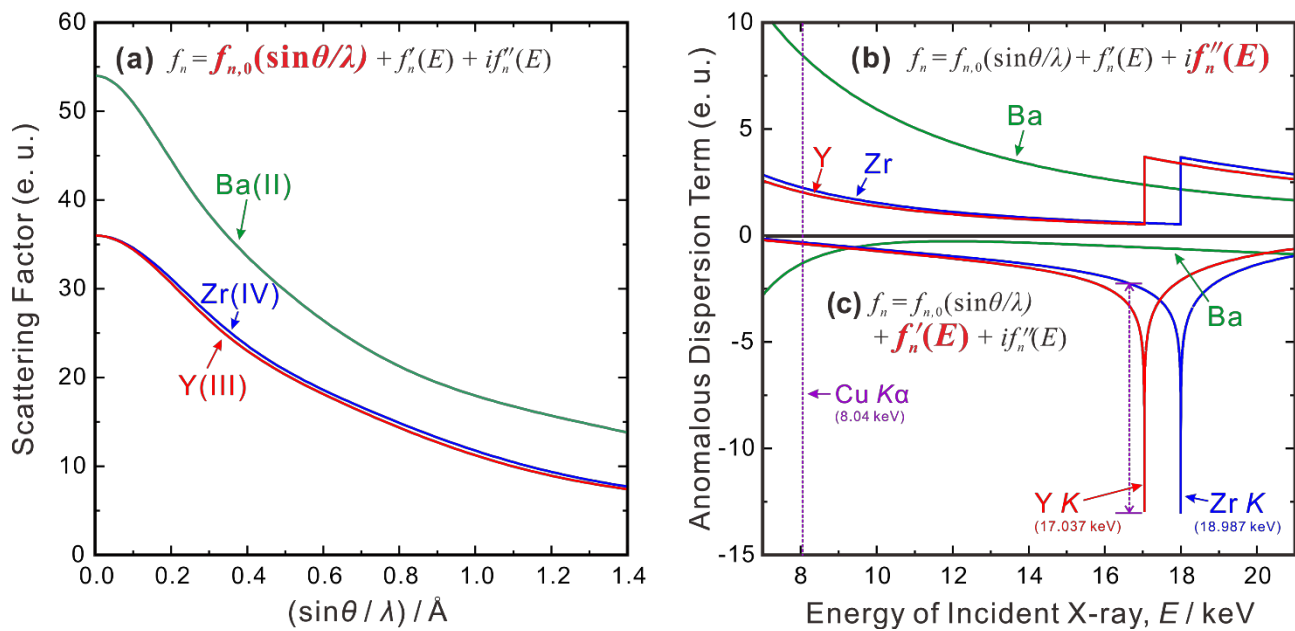
Figure 2 (a) X-ray scattering factors ($f_{n,0}(\sin\theta/\lambda)$) [20] of Ba(II), Zr(IV) and Y(III) cations, and (b)

imaginary part ($f_n''(E)$) and (c) real part ($f_n'(E)$) [21] of anomalous dispersion term of Ba, Zr, Y atoms.
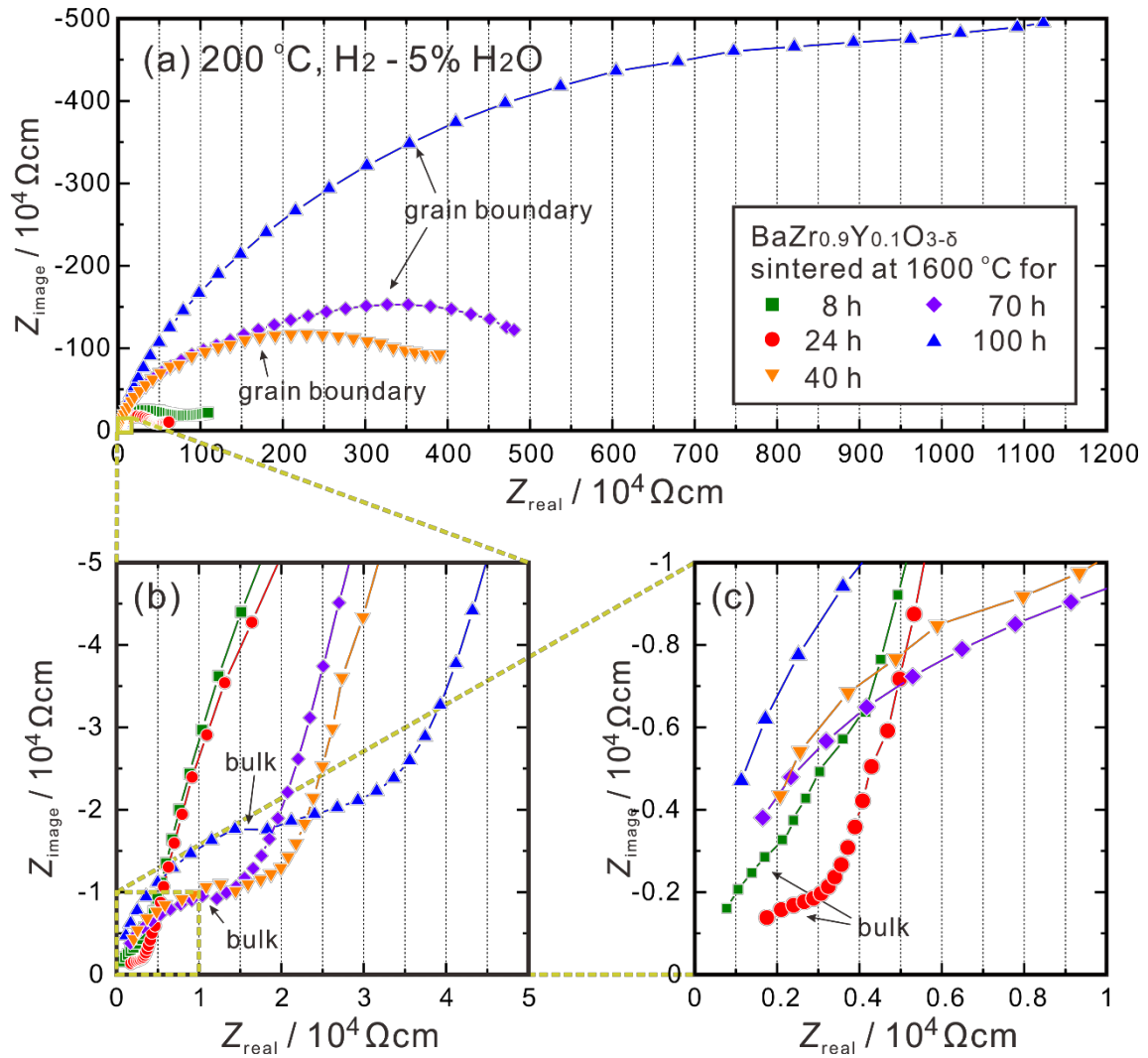
Figure 3 (a) Representative impedance spectra of $BaZr_{0.9}Y_{0.1}O_{3-\delta}$ (BZY10) collected at 200 $^\circ$C in wet H_2 (p_{H_2O} = 0.05 atm).   The samples were sintered at 1600 $^\circ$C in oxygen for 8, 24, 40, 70, and 100 h.   (b) and (c) show the magnified region where the semi-circles belonging to grain bondary and bulk resistance can be seen, respectively.
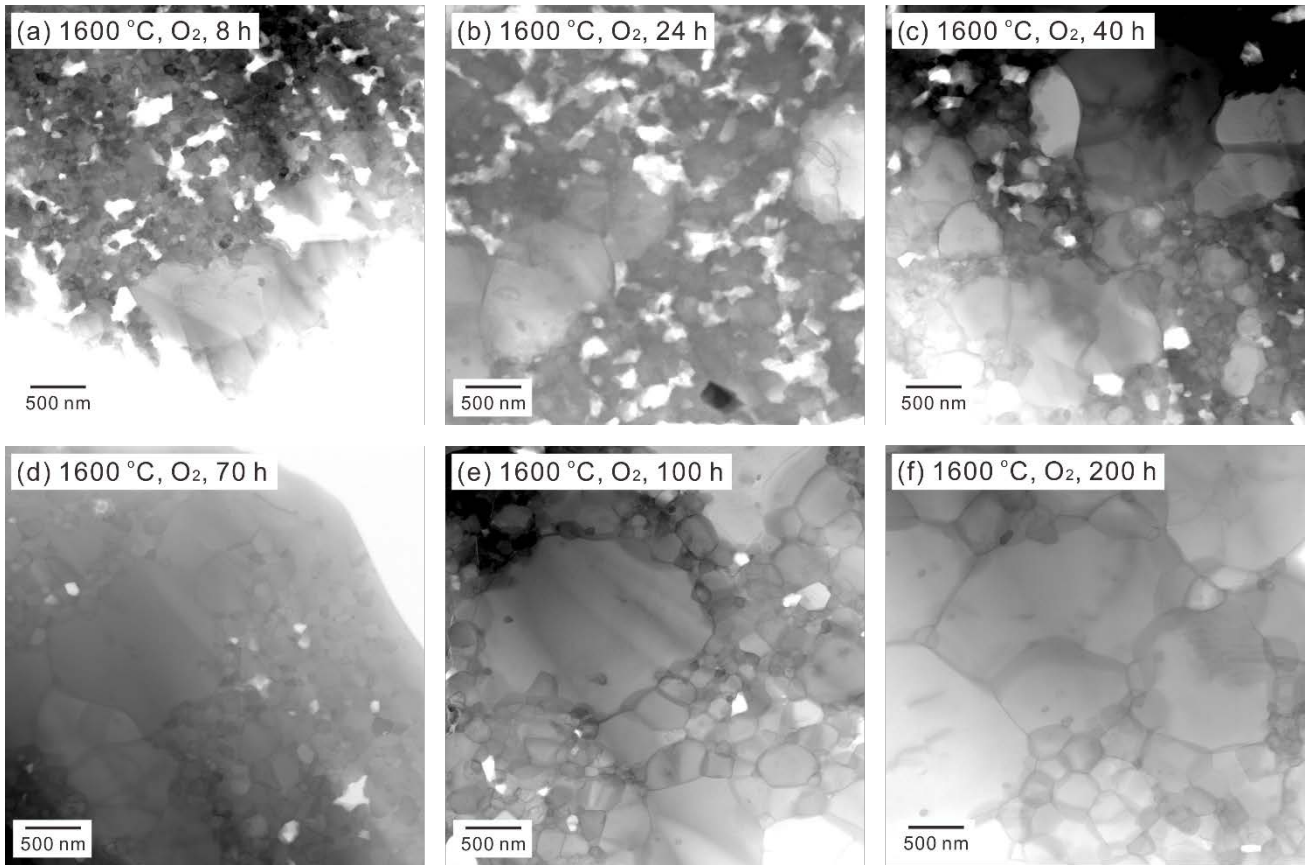
Figure 4   Bright field STEM images of BaZr$_{0.9}$Y$_{0.1}$O$_{3-\delta}$ (BZY10) sintered at 1600 ^{o}C in oxygen for

(a) 8 h, (b) 24 h, (c) 40 h, (d) 70 h, (e) 100 h, and (f) 200 h.

Figure 5 Results of STEM-EDS point analysis on composition of individual grains of $BaZr_{0.9}Y_{0.1}O_{3-\delta}$ (BZY10) sintered at 1600 °C in oxygen for (a) 8 h, (b) 24 h, (c) 40 h, (d) 70 h, (e) 100 h, and (f) 200 h. It s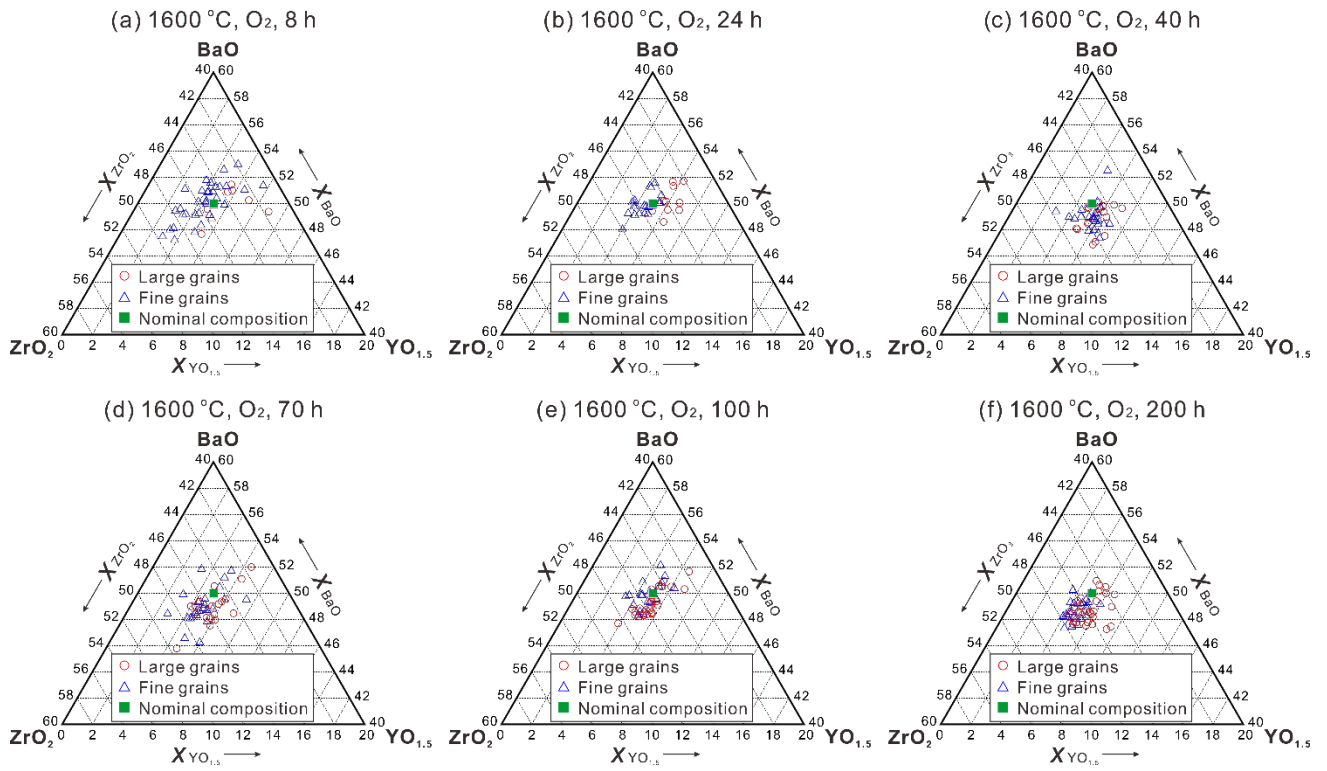hould be noted that the range of coordinate axes is not 100 at%, but 20 at% with the aim to show clear difference in composition between large and fine grains.
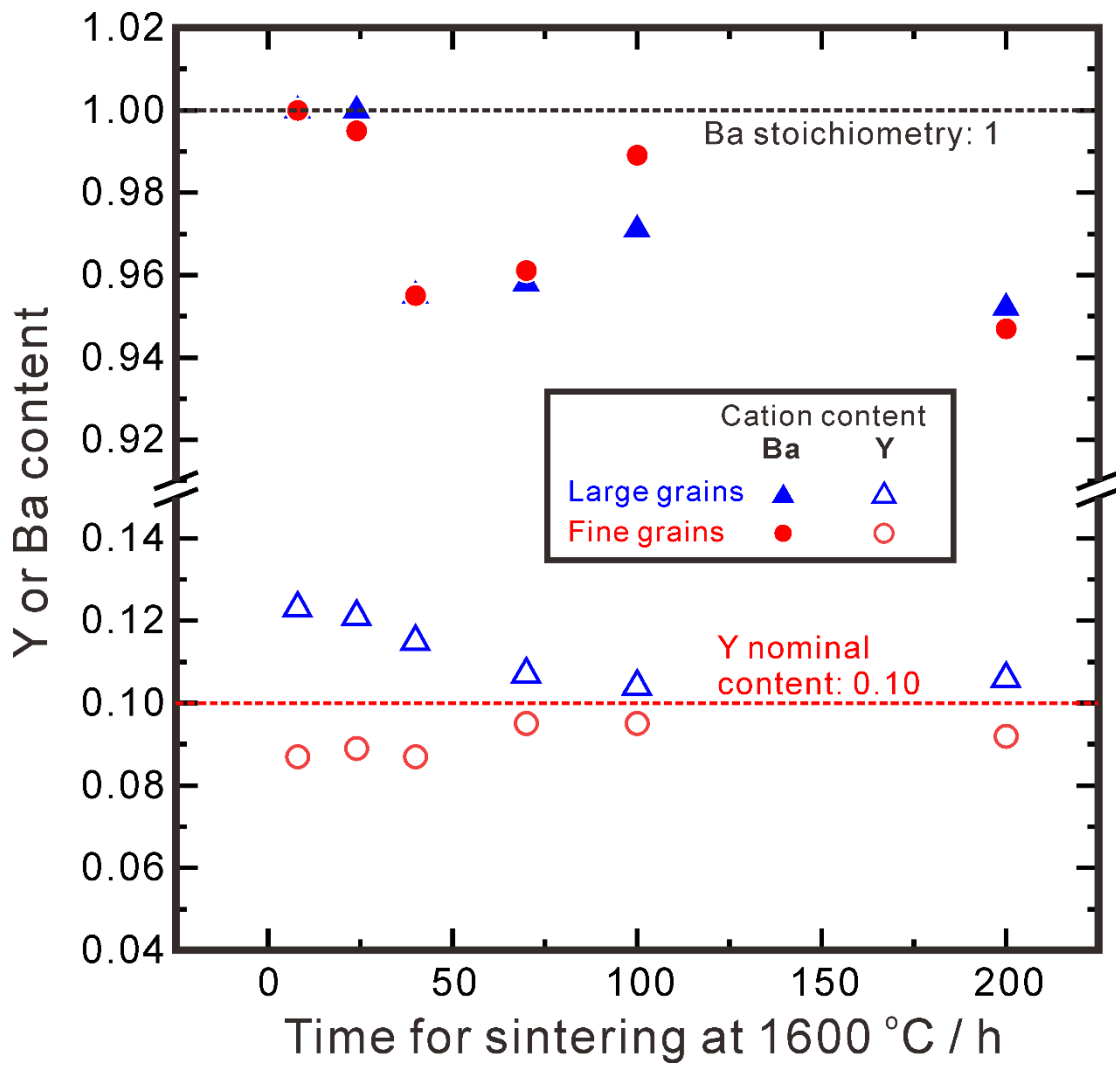
Figure 6 Content of Y or Ba of large grains and fine grains in the BZY10 samples which were sintered at 1600 $^{\circ}$C in oxygen for different time.　The values were determined by STEM-EDS point analysis.
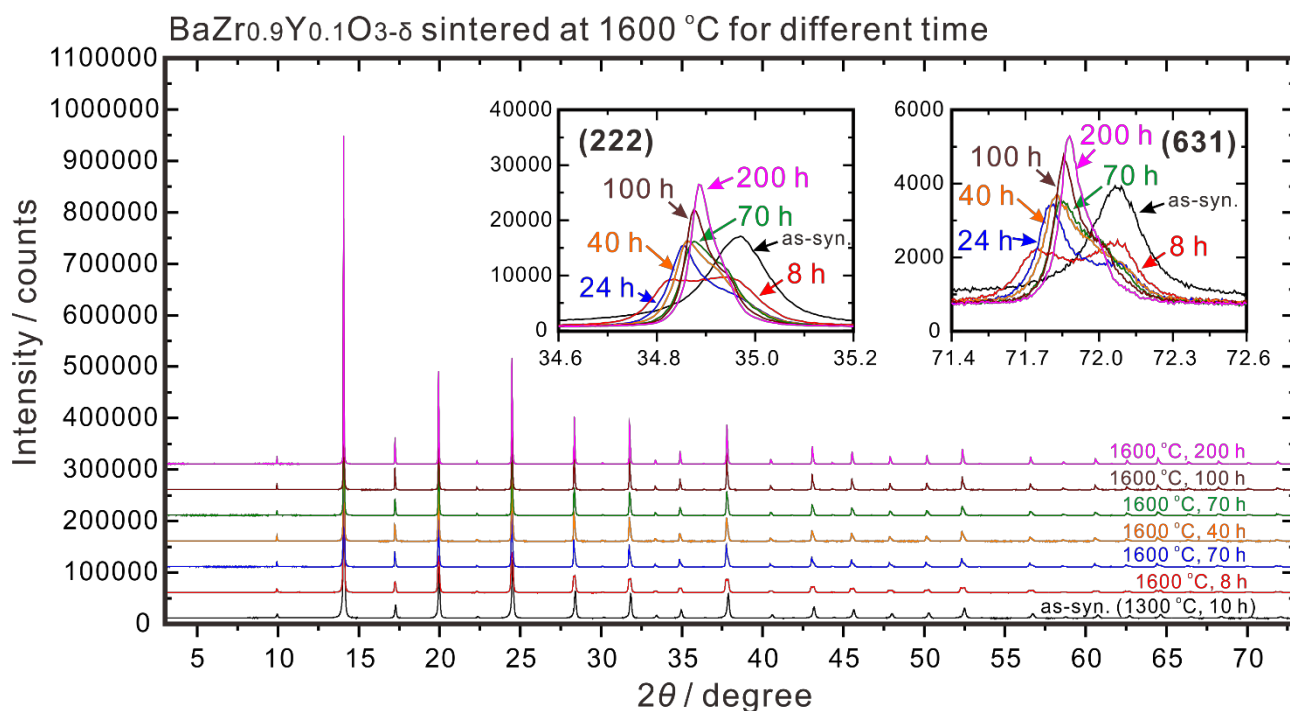
Figure 7 XRD patterns of BaZr$_{0.9}$Y$_{0.1}$O$_{3-\delta}$ collected with synchrotron radiation (17.027 keV). The samples were sintered at 1600 ^{o}C in oxygen for different time. The diffraction peaks marked as as-syn in the insets belong to the ones of the as-synthezied sample by heat-treating at 1300 ^{o}C for 10 h. And the peaks marked with time (8 – 200 h) belong to the ones of the as-sintered samples by heating at 1600 ^{o}C for relevant time. Clear shape of the (222) and (631) peaks can also be confirmed in **Figures 8** and **9**.

(222) diffraction peak of BaZr$_{0.9}$Y$_{0.1}$O$_{3-\delta}$, X-ray energy: 17.027 keV
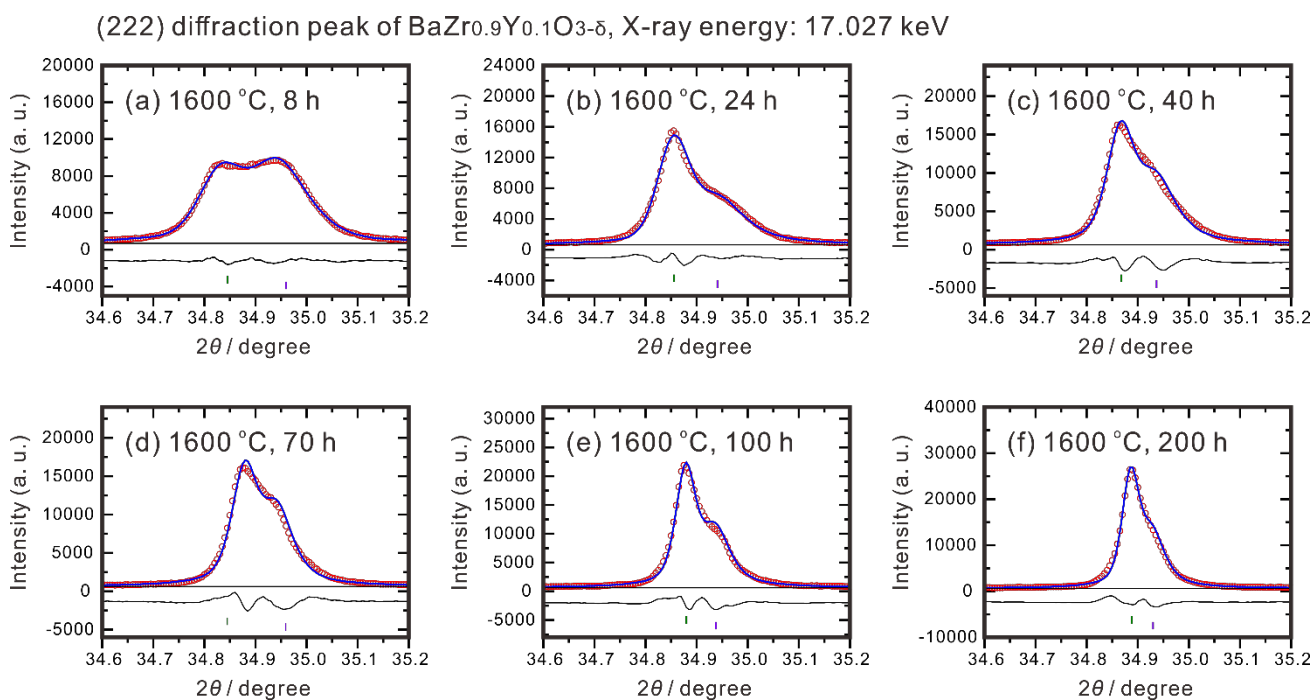
Figure 8 Rietveld refinement of the (222) diffraction peak of BaZr$_{0.9}$Y$_{0.1}$O$_{3-\delta}$ which was sintered at 1600 ^{o}C in oxygen for (a) 8 h, (b) 24 h, (c) 40 h, (d) 70 h, (e) 100 h, and (f) 200 h.   The XRD pattern was collected with synchrotron radiation (17.027 keV).   Two cubic perovskite ($Pm\overline{3}m$) structure models were adopted for the refinement.   The observed profile (red circles), calculated profile (blue), difference (black, at bottom), and Bragg peaks of the candidated phases (vertical lines) are shown.

(631) diffraction peak of BaZr$_{0.9}$Y$_{0.1}$O$_{3-\delta}$, X-ray energy: 17.027 keV

(a) 1600 °C, 8 h

(b) 1600 °C, 24 h

(c) 1600 °C, 40 h

(d) 1600 °C, 70 h

(e) 1600 °C, 100 h

(f) 1600 °C, 200 h

Figure 9 Rietveld refinement of the (631) diffraction peak of BaZr$_{0.9}$Y$_{0.1}$O$_{3-\delta}$ which was sintered at 1600 $^{\text{o}}$C in oxygen for (a) 8 h, (b) 24 h, (c) 40 h, (d) 70 h, (e) 100 h, and (f) 200 h.   The XRD pattern was collected with synchrotron radiation (17.027 keV).   Two cubic perovskite ($Pm\overline{3}m$) structure models were adopted for the refinement.   The observed profile (red circles), calculated profile (blue), difference (black, at bottom), and Bragg peaks of the candidated phases (vertical lines) are shown.
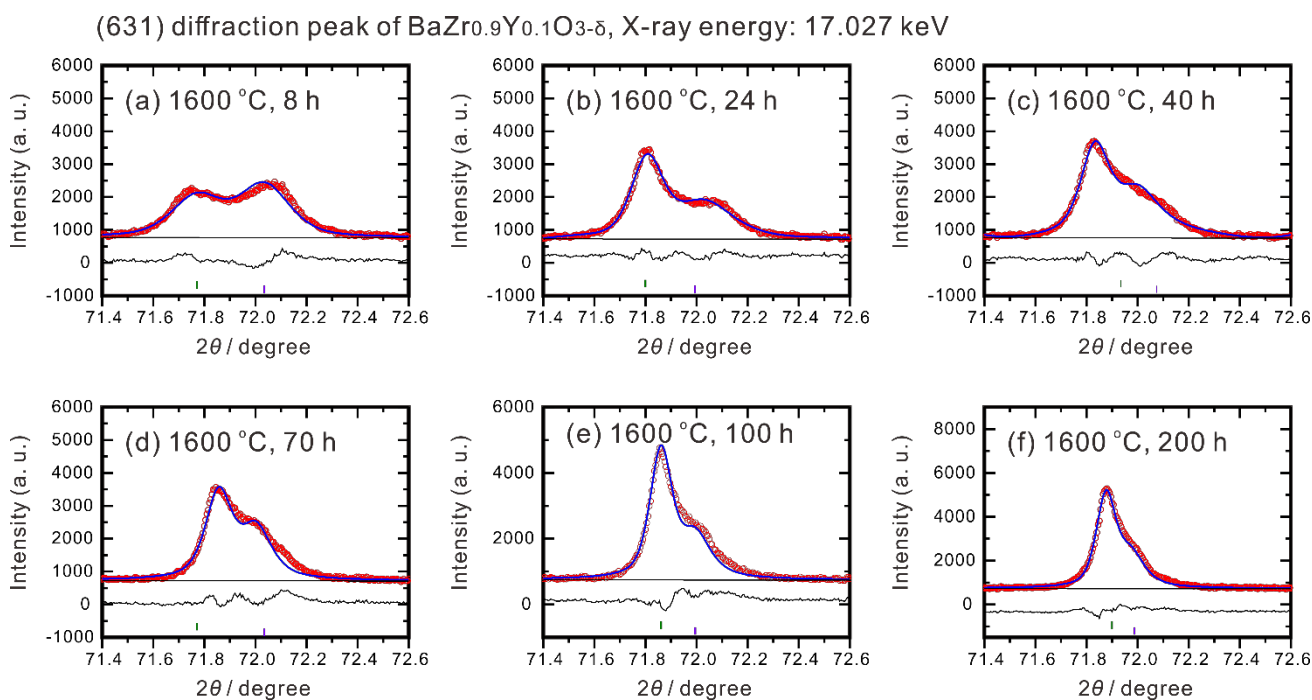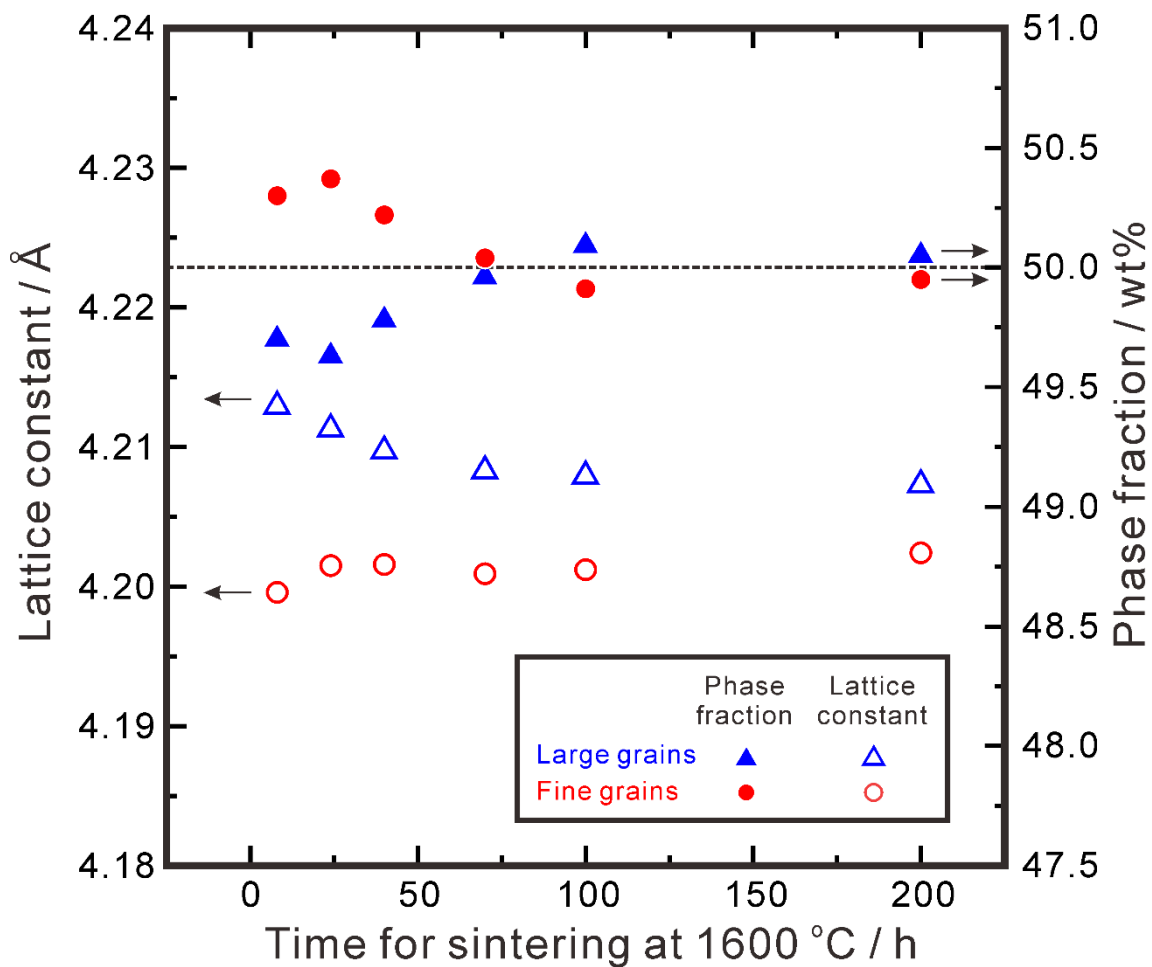
Figure 10 Lattice constants and phase fraction of large grains and fine grains in the BZY10 samples which were sintered at 1600 °C in oxygen for different time. The values were determined by analyzing the synchrotron radiation XRD patterns with Rietveld refinement.

Table 1   Information on experimental conditions for preparing the BZY10 samples.   The number corresponds to the ones in **Figure 1**.

No.	Reporter	Synthesis method	Sintering condition			Relative density / %	Atmosphere for conductivity measurement	Bulk conductivity	Microstructure (Fine grain size / Large grain size for bimodal microstructure)
			Temperature / °C	Time / h	Sacrificial powder				
1	Bohn [9]	Solid state reaction	1715	30	Unknown	97	Ar-20%O_2-4%H_2O	High	Bimodal (~ 100 nm / μm order)
2	Azad [10]	Sol-gel	1500	Unknown	Unknown	65	Ar-5%H_2-3%H_2O	High	Unknown
3	Azad [10]	Sol-gel	1500, then 1720	Unknown	Unknown	80	Ar-5%H_2-3%H_2O	Very low	Unknown
4	Azad [10]	Solid state reaction	1720	Unknown	Unknown	94	Ar-5%H_2-3%H_2O	High	Unknown
5	Kjølseth [11]	Spray pyrolysis	1650 (uniaxial hot pressing under 50 MPa)	1	No	> 95%	O_2-2.5%H_2O	Low	Uniform (~ 280 nm)
6	Kjølseth [11]	Spray pyrolysis	1600	5 min	No	> 95%	O_2-2.5%H_2O	Low	Bimodal (~ 50 nm / ~ 450 nm)
7	Duval [12]	Solid state reaction	1720	24	BZY10 powder	91	O_2-2.2%H_2O	Low	Uniform (~ 2μm)
8	Duval [12]	Solid state reaction	2200	unknown	unknown	98	O_2-2.2%H_2O	Low	Uniform (~ 5μm)
9	Han [7]	Solid state reaction	1600	24	BZY10 – 1 wt% $BaCO_3$ powder	93	H_2-5%H_2O	High	Bimodal (< 200 nm / ~ 1μm)
	This work	Solid state reaction	1600	8	BZY10 – 1 wt% $BaCO_3$ powder	89.23	H_2-5%H_2O	High	Bimodal (~ 100 nm /μm order)
	Han [8]	Solid state reaction	1600	24	BZY10 – 1 wt% $BaCO_3$ powder	92.90	H_2-5%H_2O	High	Bimodal (~ 100 nm /μm order)
				40		93.93		Low	Bimodal (~ 100 nm /μm order)
				70		94.44		Low	Bimodal (~ 200 nm /μm order)
				100		96.84		Low	Bimodal (~ 200 nm /μm order)

Table 2 Composition and relative density of $BaZr_{0.9}Y_{0.1}O_{3-\delta}$ (BZY10) sintered at 1600 °C in oxygen for 8, 24, 40, 70, 100 or 200 h.   All the samples were buried in saricificial powder composed of 99 wt% BZY10 and 1 wt% $BaCO_3$ during the heat-treatment.   The average composition was measured by ICP-AES analysis.   The local composition of intra-grain was determined by STEM-EDS point analysis on at least 44 points per sample.

Sintering condition	Average composition by ICP-AES	Local composition by STEM-EDS point analysis		Relative density / %
		Large grains	Fine grains	
1600 °C, 8 h	$Ba_{1.00}Zr_{0.90}Y_{0.10}O_{3-\delta}$	$Ba_{1.001}Zr_{0.877}Y_{0.123}O_{3-\delta}$	$Ba_{1.002}Zr_{0.913}Y_{0.087}O_{3-\delta}$	89.23
1600 °C, 24 h	$Ba_{1.00}Zr_{0.90}Y_{0.10}O_{3-\delta}$	$Ba_{1.009}Zr_{0.879}Y_{0.121}O_{3-\delta}$	$Ba_{0.995}Zr_{0.911}Y_{0.089}O_{3-\delta}$	92.90
1600 °C, 40 h	$Ba_{0.97}Zr_{0.90}Y_{0.10}O_{3-\delta}$	$Ba_{0.955}Zr_{0.885}Y_{0.115}O_{3-\delta}$	$Ba_{0.955}Zr_{0.913}Y_{0.087}O_{3-\delta}$	93.93
1600 °C, 70 h	$Ba_{0.96}Zr_{0.90}Y_{0.10}O_{3-\delta}$	$Ba_{0.958}Zr_{0.893}Y_{0.107}O_{3-\delta}$	$Ba_{0.961}Zr_{0.905}Y_{0.095}O_{3-\delta}$	94.44
1600 °C, 100 h	$Ba_{0.98}Zr_{0.90}Y_{0.10}O_{3-\delta}$	$Ba_{0.971}Zr_{0.896}Y_{0.104}O_{3-\delta}$	$Ba_{0.989}Zr_{0.905}Y_{0.095}O_{3-\delta}$	96.84
1600 °C, 200 h	$Ba_{0.95}Zr_{0.90}Y_{0.10}O_{3-\delta}$	$Ba_{0.952}Zr_{0.894}Y_{0.106}O_{3-\delta}$	$Ba_{0.947}Zr_{0.908}Y_{0.092}O_{3-\delta}$	97.10

Table 3 Results of Rietveld refinement on $BaZr_{0.9}Y_{0.1}O_{3-\delta}$ sintered at 1600 °C in oxygen for 8, 24, 40, 70, 100 or 200 h.

Sintering time / h	R_{wp} / %	χ^2	Grain type (size)	Lattice constant / Å	Fraction / wt%	Site occupancy A-site (0, 0, 0)		B-site (0.5, 0.5, 0.5)		Isotropic temperature factor / Å^2	
						Ba	Y	Zr	Y	A-site	B-site
8	6.63	3.24	Large	4.2129	49.70	1.000	0.000	0.877	0.123	0.0096	0.0027
			Small	4.1996	50.30	1.000	0.000	0.913	0.087	0.0059	0.0011
24	8.08	3.73	Large	4.2113	49.63	1.000	0.000	0.879	0.121	0.0083	0.0021
			Small	4.2015	50.37	0.995	0.000	0.911	0.089	0.0036	0.0010
40	8.24	3.89	Large	4.2097	49.78	0.955	0.000	0.885	0.115	0.0050	0.0019
			Small	4.2016	50.22	0.955	0.000	0.913	0.087	0.0042	0.0027
70	8.18	3.79	Large	4.2083	49.96	0.958	0.000	0.893	0.107	0.0044	0.0013
			Small	4.2009	50.04	0.961	0.000	0.905	0.095	0.0076	0.0051
100	7.74	3.61	Large	4.2079	50.09	0.971	0.000	0.896	0.104	0.0029	0.0008
			Small	4.2012	49.91	0.989	0.000	0.905	0.095	0.0098	0.0055
200	8.25	3.84	Large	4.2073	50.05	0.952	0.000	0.894	0.106	0.0036	0.0006
			Small	4.2024	49.95	0.947	0.000	0.908	0.092	0.0086	0.0073